Numerical Modeling of Three Types of Sensitive Clay Slope Failures

Modélisation numérique des Trois types d'argile sensible ruptures de pente

Chen Wang, Bipul Hawlader
Department of Civil Engineering, Memorial University of Newfoundland, Canada

ABSTRACT: The three major types of large-scale landslides in sensitive clay are the downhill progressive slide, flow-slide and spread. Because of strain-softening behavior of sensitive clay, the failure planes develop progressively and significant shear strain localization occurs along the failure planes (shear bands). Moreover, the failed soil mass generally displaces over a large distance. These types of landslide cannot be modeled using the commonly used limit equilibrium methods or typical finite element (FE) method developed in Lagrangian framework. In the present study, numerical simulations of these landslides—based on a large deformation FE modeling technique—is presented. The initiation of failure, formation of shear bands, global failure of the slopes, and post-failure deformation of the failed soil mass are explained. The FE simulated failure patterns compare well with the conceptual models proposed from field observation.

RÉSUMÉ: Les trois principaux types de glissements de terrain à grande échelle dans l'argile sensible sont la diapositive, le débit-slide et la propagation de descente progressive. En raison du comportement souche adoucissement d'argile sensible, les plans de rupture se développent progressivement et importante déformation de cisaillement localisation se produit le long des plans de rupture (bandes de cisaillement). En outre, la masse du sol échoué déplace généralement sur une grande distance. Ces types de glissements de terrain ne peuvent pas être modélisées en utilisant les méthodes d'équilibre limites couramment utilisés ou méthode typique éléments finis (FE) développés dans le cadre lagrangien. Dans la présente étude, les simulations numériques des thèses des glissements de terrain basés sur une grande FE modélisation de la déformation technique-est présenté. L'initiation de l'échec, la formation de bandes de cisaillement, échec global des pistes, et à la déformation post-échec de la masse du sol échoué sont expliqués. Les motifs de défaillance simulée FE se comparent bien avec les modèles conceptuels proposés par.

KEYWORDS: large-scale landslides, finite element modeling and sensitive clay.

1 INTRODUCTION

Large-scale progressive and retrogressive landslides in sensitive clays are major geohazards in eastern Canada and Scandinavia. These kind of landslides usually occur suddenly and can affect large area (>1 ha). The triggering of these landslides is attributed to natural factors (e.g. river bank erosion, earthquake and rainfall), human activities (e.g. placement of fill and pile driving) or a combination of both. Three most common types of large-scale landslides in sensitive clays are: (i) downhill progressive slides, (ii) flow-slides (sometimes called earthflows) and (iii) spreads. Figure 1 schematically shows the main features of these landslides.

Bernander and his co-workers presented a number of downhill progressive landslides in mild natural sensitive clay slopes (Bernander 2000; Bernander et al. 2016). In this type of landslide, the failure is generally initiated due to disturbance in the upslope areas and then propagates in the downslope direction over a large distance (several hundred meters in some cases, Barnander et al. (2016)). The disturbance could be resulted from construction activities such as pile driving or placement of fills. For example, Surte Landslide in Gothenburg, Sweden involved displacement of 24 ha which has been attributed to upslope pile driving. Upslope subsidence near the zone of disturbance and downslope heave are the common features of the failed soil mass (Fig. 1(a)).

The mechanisms of flow-slides are well described by Bjerrum (1955) and Tavenas (1984). In this type of landslides, multiple slides occur retrogressively (Fig. 1(b)). After the first slide, the debris gets highly remoulded and flows out leaving an unstable scarp. A second slide then occurs due to removal of the support from the soil mass in the first slide. This process continues until a final stable back scarp forms and the retrogression stops. Tavenas (1984) suggested that flow-slides might occur when: (i) an initial slide has occurred; (ii) the potential energy of the failed soil mass is high enough to remould the clay significantly; (iii) the remoulded shear strength of the clay is very low.

Finally, the spread is a type of large-scale landslide that generally triggered by erosion of soil near the toe of the slope. A quasi-horizontal failure plane forms due to toe erosion. The soil mass above this failure plane then displaces and fails successively forming a number of horsts and grabens (Cruden and Varnes 1996). The horsts are the blocks of intact clay having a sharp wedge pointing upward, while the grabens are the blocks having a flat horizontal top surface (Fig. 1(c)).

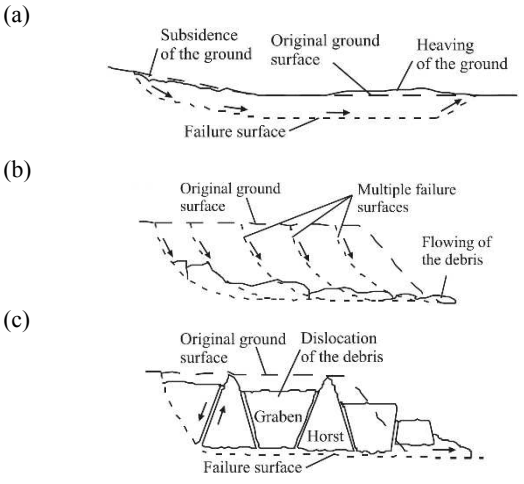

Figure 1. Three common types of large-scale landslides in sensitive clays: (a) downhill progressive slide; (b) flow-slide; (c) spread. (after Locat et al. 2011)

Because of strain-softening behavior of sensitive clays, the failure surfaces develop progressively. Moreover, a massive volume of soil mass displaces in these types of landslides. Unfortunately, the limit equilibrium methods commonly used in slope stability analysis cannot explain the progressive development of failure. Moreover, the complete failure process cannot be modeled using the typical FE methods developed in

Lagrangian framework because of significant mesh distortion and numerical issues. Therefore, conceptual or simplified models have been proposed in the past to explain such landslides (Bernander et al. 2016; Locat et al. 2011).

The objective of this study is to present large deformation FE modeling of sensitive clay slope failures. This method has been previously used by the authors and their co-workers for successful simulation of spreads (Dey et al. 2015; Wang et al. 2016). In the present study, simulations are performed for varying geometries, soil properties and triggering factors to simulate all three types of failure shown in Fig. 1.

2 PROBLEM DEFINITION

The simulation results of 3 cases are presented in this paper to explain the mechanisms involved in downhill progressive slides, flow-slides and spreads. The simulations are performed for plane strain condition. In Case-I, a mild slope (β=3°) is considered to model downhill progressive failure (Fig. 2(a)). The peak undrained shear strength (s_{up}) of the top 20 m thick sensitive clay layer is 35 kPa. There is a change in slope angle at the point X in the downslope area (Fig. 2(a)). Bernander et al. (2016) showed that the downslope areas also could have a very mild slope. However, for simplicity the downslope area is assumed to be horizontal. The soil below the sensitive clay (base layer) is considered as a strong material. An embankment of 7.5 m height and 23 m crest width is placed in the upslope area at 200 m from point X. To triggers the landslide, the embankment load is gradually applied by increasing the unit weight of the fill.

In Case-II, a 30 m high riverbank slope of sensitive clay is studied. The slope angle β is 26.6° (2H:1V) and the upslope area is horizontal. The s_{up} of the sensitive clay layer increases linearly from 60 kPa at the ground surface to 110 kPa at the bottom of the sensitive clay layer. Again, a 10 m strong base layer is considered below the sensitive clay layer. The failure is triggered by toe erosion which is the most common triggering factor for the landslides in eastern Canada. In Case-III, the geometry of the slope is same as in Case-II but a 5 m crust above the sensitive clay layer is considered. The peak undrained shear strength of the sensitive clay layer increases linearly with depth from 40 to 100 kPa.

In all three cases, the mobilized shear strength of the sensitive clay layer (s_u) decreases with plastic deformation and sensitivity (S_t) as discussed in Section 3.2.

3 FINITE ELEMENT MODELING

3 .1 *Numerical technique*

Coupled Eulerian-Lagrangian (CEL) technique available in Abaqus FE software is used. In CEL, the Eulerian material (soil) can flow through the fixed mesh. Therefore, there is no numerical issue related to mesh distortion or mesh tangling even at large strains around the failure planes. The performance of CEL technique of simulating sensitive clay slope failure has been discussed in previous studies (Dey et al. 2015, 2016a,b; Wang et al. 2016). The FE model consists of two parts: (i) soil, (ii) void space to accommodate displaced soil mass (Fig. 2). The soil is modeled as Eulerian material using the EC3D8R elements in Abaqus, which are 8-noded linear brick, multi-material, reduced integration elements. Soil and void spaces are created in Eulerian domain using Eulerian Volume Fraction (EVF) tool. For void space EVF is zero (i.e. no soil). On the other hand, EVF is unity inside the slope geometry, which means these elements are filled with Eulerian materials (i.e. soils).

Only three-dimensional model can be generated in CEL. In the present study, the model is only one element thick in the out of plane direction. The movement of soil perpendicular to the x-y plane in Fig. 2 is restricted by applying zero velocity boundary condition in order to mimic plane strain condition. All velocity components are zero at the bottom and left vertical planes. At the right vertical plane, zero velocity boundary condition is applied from the bottom to the ground surface. However, in the void space no velocity boundary condition is applied such that the debris can flow out of the domain as shown in the following sections. This also reduces the computational cost because the model size in downslope area could be reduced. No boundary condition is applied at the soil–void interface so that the soil can move into the void space when displaced. Cubical elements of 0.3 m size are used in all the simulations.

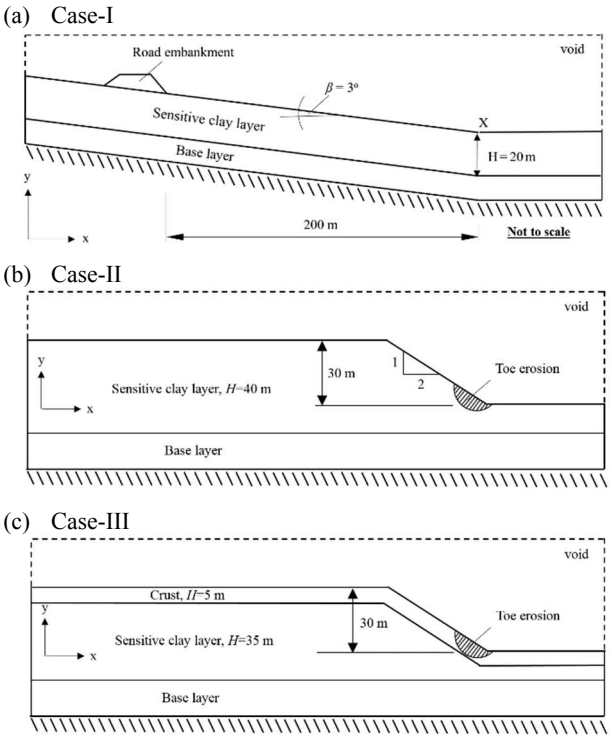

Figure 2. Geometry of the slope used in numerical analysis

The numerical analysis consists of three steps of loading. In the first step, geostatic load is applied to bring the slope in in-situ stress condition. The slopes are stable under geostatic load. In the second step, the triggering factors (e.g. upslope construction in Case-I and toe erosion in Cases II and III) are applied to initiate the landslide. In the final step, analyses continue for a period of time without any increase of external load to observe the post-slide behaviour.

3 .2 *Soil parameters*

The analyses are performed for undrained condition because landslides in sensitive clays usually occur in a very short time period.

Sensitive clays show post-peak softening behavior in undrained loading (Tavenas et al. 1984; Quinn 2011). The mobilized undrained shear strength after the peak (s_u) can be related plastic shear strain or post-peak displacement (δ). In this study, the softening behavior of sensitive clays is defined using the following exponential relationship.

$$s_u = \left[\frac{1}{S_t} + \left(1 - \frac{1}{S_t}\right) e^{-3\delta/\delta_{95}}\right] s_{up} \qquad [1]$$

where, s_u is the mobilized undrained shear strength at displacement δ; S_t is the sensitivity of the soil; $\delta=\delta_{total}-\delta_p$; δ_p is

the displacement required to attain the peak undrained shear strength s_{up}; and δ_{95} is the value of δ at which the undrained shear strength of the soil is reduced by 95% of (s_{up}-s_{uR}). Equation (1) is a modified form of strength degradation equation proposed by Einav and Randolph (2005) but in terms of displacement. The authors discussed the model parameters required in this equation and its application in modeling sensitive clay slope in previous studies (Dey et al. 2015, 2016a,b; Wang et al. 2016).

Figure 3 shows the relationship between the shear strength and shear displacement. Line oa represents a linear elastic pre-peak behavior. s_{up} is mobilized at point a and remains constant up to point b for a displacement of δ_{pc}. The curve bcd is defined by Eq. (1). After s_{uR}, the shear strength reduces slowly with shear displacement. The reduction of s_u in this zone is defined by a linear line de from s_{uR} to s_{uld} at a large displacement. After that, s_u remains constant (s_u=s_{uld}). The geotechnical parameters used for modeling sensitive clay are shown in Table 1.

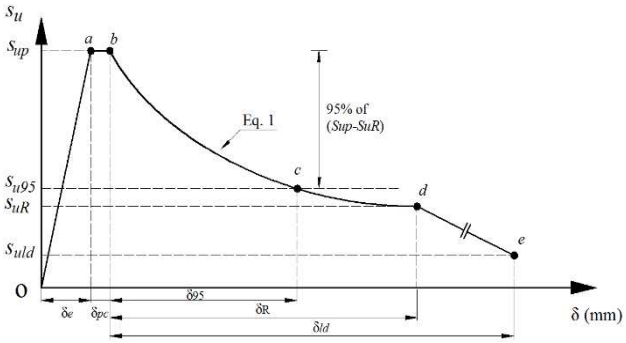

Figure 3. Stress–displacement behavior of sensitive clay

The base layer is modeled as elastic material with Young's modulus E=200 MPa. The crust in Case-III is modeled as elastic-plastic material without softening using the following geotechnical parameters: s_u=50 kPa, E_u=10 MPa (=200s_u) and ν_u=0.495.

Table 1: Parameters used for modeling sensitive clay

Soil Parameters	Case-I	Case-II	Case-III
Undrained Young's modulus, E_u (MPa)	10	10	10
Poisson's ratio, ν_u	0.495	0.495	0.495
Peak undrained shear strength, s_{up} (kPa)	35	60-110	40-100
Residual undrained shear strength, s_{uR} (kPa)	s_{up}/5	s_{up}/3	s_{up}/5
Large displacement undrained shear strength, s_{uld} (kPa)	s_{up}/50	s_{up}/50	s_{up}/35
Unit weight of soil, γ (kN/m^3)	18.0	18.0	18.0
Plastic shear displacement for 95% degradation of soil strength, δ_{95} (mm)	30	30	30
Plastic shear displacement for initiation of softening, δ_{pc} (mm)	2	3	3
Plastic shear displacement for large displacement undrained shear strength, δ_{ld} (mm)	2000	500	2000

4 FINITE ELEMENT RESULTS

4 .1 *Case-I: Downhill progressive slide*

This case demonstrates a downhill progressive slide induced by embankment construction. The equivalent plastic strain (PEEQVAVG) obtained from Abaqus is used to examine the formation of shear bands. Before placing the embankment, the shear stress in soil elements increases with depth due to self-weight of the soil. The shear stress at the bottom of the sensitive clay layer (τ_0) can be calculated as τ_0=γHsinβ. In this case, for γ=18 kN/m^3, H=20 m and β=3°, the value of τ_0 is 18.8 kPa, which is less than s_{up} (=35 kPa) of the soil. Therefore, development of any plastic shear strain or failure of the slope is not expected under gravity load.

In the second step, the external load from the embankment induces additional shear stress in the sensitive clay layer and triggers the failure. Figure 4(a) shows that the failure initiates below the embankment from point A which is located at the boundary between sensitive clay and base layers. Figure 4(b) shows the failure pattern at the end of second step. The shear band then propagates mainly in downslope direction from point A. Although no additional external load is applied in the third step, the propagation of shear band continues with time because s_u reduces with accumulation of plastic shear strains in the failure planes that causes redistribution of additional loads to the surrounding soil elements. Figure 4(c) shows that the shear band propagates downhill along the bottom of the sensitive clay layer and finally reach the toe of the slope. As the failure continues, the soil around the embankment subsides and the soil near the toe of the slope heaves forming a number of inclined shear bands in the sensitive clay layer, which indicates compressive failure in this area (Fig. 4(d)).

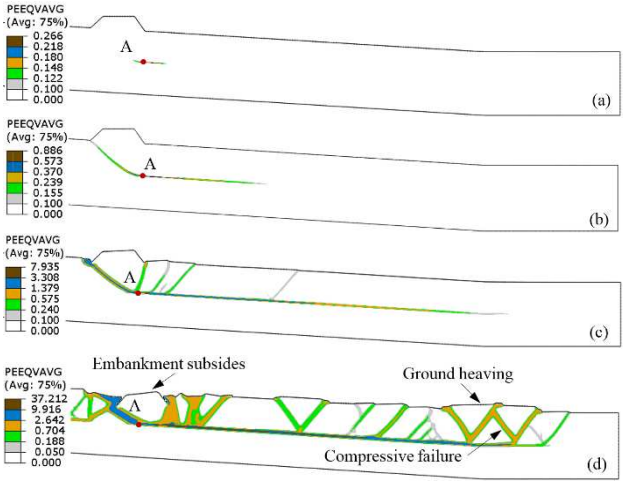

Figure 4. FE simulation of downward progressive failure (Case-I)

4 .2 *Case-II: Flow-slide*

This case demonstrates a flow-slide near a river bank triggered by toe erosion. The slope is stable after the gravity step. In the second step, the shear strength of the soil in the eroded zone (hatched area in Fig. 2(b & c)) is reduced to 1 kPa, which causes the failure of this soil block and spreads over a large area. This phenomenon is similar to the toe erosion at river banks in the field, the failed block might be displaced a large distance in the downslope or eroded by river flow. Figure 5(a) shows that, due to removal of a small soil block near the toe, a horizontal shear band forms in the sensitive clay layer and then propagates up to the ground surface causing a global failure. The horizontal segment of the shear band is located at 10 m above the interface between sensitive clay and base layers. This implies that the location of shear band is not predefined rather it forms at critical location depending upon the kinematics of problem. Therefore, the present study could eliminate the a priori definition of the failure planes as used in previous studies for modeling sensitive clay slopes (Locat et al. 2011, Quinn et al. 2011). With displacement, the failed soil mass breaks into pieces through formation of a number of shear bands within it. When debris move sufficiently large distance, the support on the intact soil reduces that causes the second rotational slide. The depth of this slide is less than that of first slide. Similar

phenomenon has been observed in the field in flow-slides (Demers et al. 2014). The failure process continues as shown in Figs. 5(b)-5(d). Finally, the failure stopped after the fourth slide because the back scarp is shallow and is not steep enough for causing global failure of another soil mass.

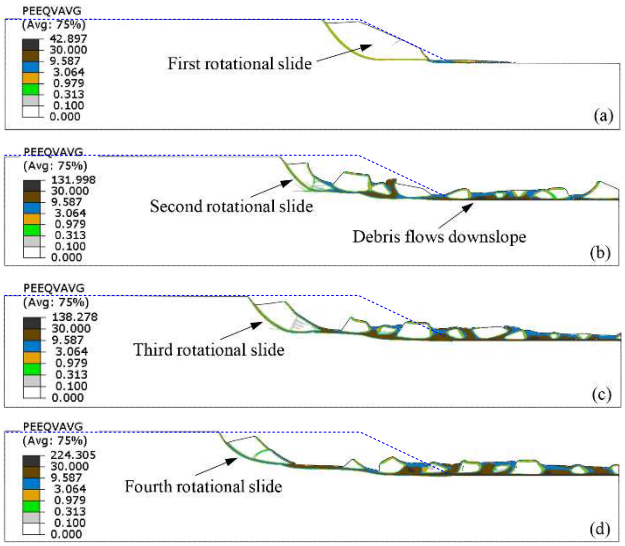

Figure 5. FE simulation of flow-slide (Case-II)

4 .3 *Case-III: Spread*

The modeling of a spread initiated by toe erosion near the river bank is presented in this section. Similar to Case-II, the slope is stable under in-situ stress condition. Toe erosion reduces the support and trigger slope failure by formation of a horizontal shear band in the sensitive clay layer (Fig. 6(a)). As the soil above the shear band displaces to the right, s_u in the shear band reduces because of plastic deformation (see Fig. 3). At one stage curved upward shear bands form from the horizontal one and cause global failure (Fig. 6(b)). The propagation of the horizontal shear band continues and the soil mass above the horizontal shear band fails progressively. A number of horsts and grabens, similar to Fig. 1(c), are formed (Fig. 6(c)). A close examination of the simulation results show that the presence of the crust and slow movement of the failed soil blocks, as compared to Case II, are the potential causes of formation of horsts and grabens instead of flow-slide as presented in Fig. 5.

5 CONCLUSIONS

Three typical large-scale landslides in sensitive clays are simulated. Using a large deformation FE modeling technique in Abaqus, the mechanisms involved in these landslides—triggering, shear bands formation, soil mass dislocation and large displacement of debris—are examined. The simulation results are comparable to the conceptual model proposed in previous studies based on post-failure observation. It is shown that the variation of geometry of the slope, soil properties and triggering factors could change the failure pattern.

Case-I shows that an upslope loading could create a long shear band and cause a large landslide of a mild natural sensitive clay slope as observed in the field. Case-II and Case III show that a small slide/erosion near the toe of river bank could cause large landslides. Depending on mobility of the failed soil mass, the failure could be spread or flow-slide.

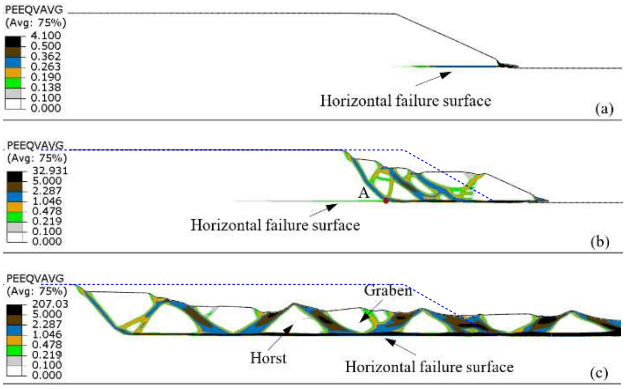

Figure 6. FE simulation of spread (Case-III)

6 ACKNOWLEDGEMENTS

The financial support from the Research and Development Corporation of Newfoundland and Labrador, NSERC and MITACS is greatly acknowledged.

7 REFERENCES

Bernander S. 2000. Progressive landslides in long natural slopes, formation, potential extension and configuration of finished slides in strain-softening soils. Licentiate thesis, *Department of Civil and Mining Engineering, Luleå University of Technology*, Luleå, Sweden.

Bernander S., Kullingsjo A., Gylland A.S., Bengtsson P., Knutsson S. Pusch R., Olofsson J. and Elfgren L. 2016. Downhill progressive landslides in long natural slopes: triggering agents and landslide phases modeled with a finite difference method. *Canadian Geotechnical Journal* 53 (10), 1565-1582.

Bjerrum L. 1955. Stability of natural slopes in quick clay. *Géotechnique* 5 (1), 101-119.

Cruden D.M. and Varnes D.J. 1996. Landslides types and processes. In Landslides investigation and mitigation. Special Report 247. *Transportation Research Board, National Research Council*. Washington, D.C. 37-75.

Demers D., Robitaille D., Locat P. and Potvin J. 2014. Inventory of large landslides in sensitive clay in the province of Quebec, Canada: preliminary analysis. *Advances in Natural and Technological Hazards Research*. 36, 77-89.

Dey R., Hawlader B., Phillips R. and Soga, K. 2015. Large deformation finite element modeling of progressive failure leading to spread in sensitive clay slopes. *Géotechnique*, 65 (8), 657-668.

Dey R., Hawlader B., Phillips R. and Soga K. 2016a. Modeling of large deformation behaviour of marine sensitive clays and its application to submarine slope stability analysis. *Canadian Geotechnical Journal*, 53 (7), 1-18.

Dey, R., Hawlader, B., Phillips, R. and Soga, K. 2016b. Numerical modelling of submarine landslides with sensitive clay layers. *Géotechnique*, 66 (6), 454-468.

Einav I. and Randolph M.F. 2005. Combining upper bound and strain path methods for evaluating penetration resistance. *International Journal of Numerical Methods Engineering*, 63 (14), 1991-2016.

Locat A., Leroueil S., Bernander S., Demers D., Jostad H.P. and Ouehb L. 2011. Progressive failures in eastern Canadian and Scandinavian sensitive clays. *Canadian Geotechnical Journal* 48 (11), 1696-1712.

Tavenas F. 1984. Landslides in Canadian sensitive clays - a state of the art. *In Proceedings of the 4th International Symposium on Landslides*, Toronto, Ontario, 141-153.

Quinn P.E., Diederichs M.S., Rowe R.K. and Hutchinson D.J. 2011. A new model for large landslides in sensitive clay using a fracture mechanics approach. *Canadian Geotechnical Journal*, 48(8), 1151-1162.

Wang C., Hawlader B. and Perret D. 2016. Finite element simulation of the 2010 Saint-Jude landslide in Quebec. *In: Proceedings of the 69th Canadian Geotechnical Conference*, Quebec City, Quebec, Canada.